Journal of Reproduction and Development, Vol. 65, No 2, 2019

—Original Article—

Behavior of ACRBP-deficient mouse sperm in the female reproductive tract

Kiyoshi NAGASHIMA[1, 2)*], Tomoyuki USUI[2)*] and Tadashi BABA[1–3)]

[1)]*Ph.D. Program in Human Biology, School of Integrative and Global Majors, University of Tsukuba, Ibaraki 305-8577, Japan*
[2)]*Faculty of Life and Environmental Sciences, University of Tsukuba, Ibaraki 305-8572, Japan*
[3)]*Life Science Center for Survival Dynamics, Tsukuba Advanced Research Alliance (TARA), University of Tsukuba, Ibaraki 305-8577, Japan*

Abstract. Gene-knockout mice lacking ACRBP, a proacrosin-binding protein localized in the acrosome of sperm, have been shown to exhibit male subfertility, owing to abnormal formation of the acrosome. In this study, to elucidate the mechanism contributing to the subfertility phenotype, we examined the behavior of ACRBP-deficient mouse sperm in the female reproductive tract. When sperm that had migrated into the uterus and oviduct after mating were counted, the number of ACRBP-deficient sperm was noticeably smaller in the oviduct of mice post mating. However, ACRBP-deficient sperm recovered from the oviduct possessed morphologically normal head shape and retained normal motility. Importantly, ACRBP-deficient sperm displayed a marked reduction in the ability to successfully gain access to unfertilized oocytes. These data suggest that male subfertility of ACRBP-deficient mice may be attributed to incompleteness of the acrosome reaction rather than impairment in sperm migration from the uterus to the oviduct.
Key words: ACRBP, Female reproductive tract, Fertilization, Mouse, Sperm

(**J. Reprod. Dev. 65:** 97–102, 2019)

ACRBP [1–3] is a binding proitein specific for the precursor (proACR) and intermediate forms of the serine protease ACR [4] localized in the acrosome of mammalian sperm. Porcine, guinea pig, and human spermatogenic cells produce only a single form of *Acrbp* (termed *Acrbp-W*) mRNA, whereas two mRNA forms, wild-type *Acrbp-W* and intron 5-retaining variant *Acrbp-V5* mRNAs, are synthesized by pre-mRNA alternative splicing of the *Acrbp* gene in mouse [3]. Gene-knockout mice lacking both ACRBP-W and ACRBP-V5 (*Acrbp*$^{-/-}$) showed male subfertility, owing to abberant formation of the acrosome [3]. Further experiments on transgenic mice exogenously expressing either one of these two ACRBPs demonstrated that ACRBP-V5 plays the key role in the formation and configuration of an acrosomal granule into the center of the acrosomal vesicle during early spermiogenesis. The major role of ACRBP-W is to retain the inactive status of proACR in the acrosome, in addition to the promotion of ACR release from the acrosome during acrosomal exocytosis [1–3].

Acrbp$^{-/-}$ mouse epididymal sperm have been reported to exhibit a continuous variation in the shapes of the acrosome and nucleus [3]. The whole population of *Acrbp*$^{-/-}$ mouse sperm was grouped into four types in the preceding study [3] (types 1, 2, 3, and 4), and no obvious difference was found between wild-type (*Acrbp*$^{+/+}$) and type-1 *Acrbp*$^{-/-}$ mouse sperm. Nuclear shape of the type-1 mutant mouse sperm is similar to that of *Acrbp*$^{+/+}$ mouse sperm, despite the fact that its acrosome is partially fragmented on the head or is not fully elongated at the dorsal edge. The nuclei of type-2 and type-3 *Acrbp*$^{-/-}$ mouse sperm are moderately and severely affected, respectively, in addition to the fragmented structure of the acrosome. Moreover, similar to GOPC- [5], ZPBP1- [6], and SPACA1-null sperm [7], type-4 *Acrbp*$^{-/-}$ mouse sperm display both fragmented acrosome and round-headed shape with a coiled midpiece around the deformed nucleus [3]. On the other hand, live-imaging analysis indicated that type-1 and type-2 *Acrbp*$^{-/-}$ mouse sperm exhibit irregular patterns of flagellar beating and head rotations. Flagellar beating of type-3 sperm is considerably dysfunctional, while type-4 sperm display no forward movement [3]. Thus, impaired formation of acrosomal granules in *Acrbp*$^{-/-}$ mouse spermatogenic cells results in the fragmented structure of the acrosome, which is linked to the abnormally condensed nuclear structure and the diminished motility of *Acrbp*$^{-/-}$ mouse sperm.

According to currently accepted concepts regarding the behavior of ejaculated mouse sperm in the female reproductive tract [8–12], the transport of sperm from the uterus to the middle region of the oviduct via the uterotubal junction is highly dependent on oviductal fluid flows generated by myosalpinx contractions. Motility of sperm is required for its migration from the middle oviductal region to the ampulla [10]. Importantly, fertilizing sperm mostly initiate the acrosome reaction at least in the upper isthmus region before reaching the unfertilized oocytes in the ampulla. As described above, *Acrbp*$^{-/-}$ male mice show a severely reduced fertility; even when female mice that previously mated with the *Acrbp*$^{-/-}$ males become pregnant, the litter sizes are

Received: November 22, 2018
Accepted: December 6, 2018
Published online in J-STAGE: December 29, 2018

Correspondence: T Baba (e-mail: baba.tadashi.gf@u.tsukuba.ac.jp)
*K Nagashima and T Usui contributed eqally to this work.

greatly decreased [3]. The mechanism contributing to the subfertility phenotype is of particular interest, because *Acrbp*$^{-/-}$ mouse sperm display a continuous variation of structural and functional features. We, therefore, examined the behavior of *Acrbp*$^{-/-}$ mouse sperm in the female reproductive tract.

Materials and Methods

Mice

Acrbp$^{-/-}$ mice were generated as described previously [3], backcrossed to ICR mice (Japan SLC, Hamamatsu, Shizuoka, Japan), and maintained in our laboratory. A transgenic mouse line, B6D2F1-Tg (CAG/su9-DsRed2, Acr3-EGFP) RBGS002Osb [13], was obtained from RIKEN BioResource Center with the permission of Drs M Okabe and M Ikawa, maintained in our laboratory, and crossed with *Acrbp*$^{-/-}$ mice. The *Tg*$^{+/-}$/*Acrbp*$^{+/-}$ F1 mice were further mated with *Acrbp*$^{-/-}$ mice to produce *Tg*$^{+/-}$/*Acrbp*$^{-/-}$ F2 mice. Mice were genotyped for *Acrbp* and *Tg* mutations by polymerase chain reaction (PCR) analysis of tail DNAs using the following sets of primers: *Acrbp,* 5'-GTATCCCTTGGACCACTGAAC-3' and 5'-GATCCAACTGAACGAGAGTGG-3'; *Acrbp* null-mutation, 5'-GTATCCCTTGGACCACTGAAC-3' and 5'-CACTTGTGTAGCGCCAAGTGC-3'; *CAG/su9-DsRed2* integration, 5'-CCTACAGCTCCTGGGCAACGTGC-3' and 5'-AGCCAGAAGTCAGATGCTCAAGGGGC-3'; *Acr3-EGFP* integration, 5'-GTGGAGCTTTGTGAGGTCACAG-3' and 5'-CAGCTTGCCGGTGGTGCAGATG-3'. All animal experiments were carried out in compliance with relevant Japanese and institutional laws and guidelines, and were approved by the University of Tsukuba Animal Ethics Committee (authorization numbers: 16-030, 17-002, and 18-352).

Sperm migration in the female reproductive tract after mating

ICR-strain mice (8 weeks old; Japan SLC) were superovulated by intraperitoneal injection of pregnant mare's serum gonadotropin (5 units; ASKA Pharmaceutical, Tokyo, Japan) followed by human chorionic gonadotropin (hCG; 7.5 units; ASKA Pharmaceutical) 48 h later, as described previously [14, 15]. Superovulated female mice were mated with 3-month-old males 12 h after hCG injection. Sperm were recovered from the uterus 1.5 h after mating, transferred into a 1.5-ml microtube, diluted with phosphate-buffered saline (PBS), and counted under an IX-71 microscope (Olympus, Tokyo, Japan). The oviducts were carefully excised from the mice 2 h after mating, placed on petri dishes, and perfused with PBS (50 µl). Sperm were then counted as described above. When the superovulated females were mated with *Tg*$^{+/-}$/*Acrbp*$^{+/+}$ or *Tg*$^{+/-}$/*Acrbp*$^{-/-}$ mice, the intact oviduct connected to the uterus, ovary, and fat pad was pulled out from the mice 6 h after mating, placed on a glass slide, and directely observed at 37°C under an IX-71 fluorescence microscope (Olympus), as described previously [10].

Morphological analysis

Cauda epididymal sperm were dispersed in a 50-µl drop of TYH medium [16] free of bovine serum albumin (BSA) for 10 min, and capacitated by incubation for 2 h in a 0.2-ml TYH drop at 37°C under 5% CO_2 in air. Superovulated female mice were mated with males, as described above. Sperm were recovered from the uterus and oviduct 1.5 and 4 h after mating, respectively. Epididymal, uterine, and oviductal sperm were fixed with 4% paraformaldehyde in ice-cold PBS for 30 min, washed with PBS, treated with PBS containing 3% normal goat serum for 30 min, incubated with Alexa Fluor 568-conjugated peanut agglutinin (PNA; 3 µg/ml; Thermo Fisher Scientific, Waltham, MA, USA), MitoTracker Green FM (2.5 µg/ml; Molecular Probes, Eugene, OR, USA), and Hoechst 33342 (2.5 µg/ml; Thermo Fisher Scientific) for 30 min, washed with PBS, mounted, and then observed under an IX-71 fluorescence microscope (Olympus), as described previously [17].

Sperm motility

Sperm were video-recorded on a 37°C-warm plate at 200 frames per sec under an IX-71 phase-contrast microscope (Olympus) equipped with an HAS-220 high-speed camera (DITECT, Tokyo, Japan). Trajectories of sperm were analyzed using the Manual Tracking plugin of ImageJ software (http://rsbweb.nih.gov/ij/). The apical end of sperm head was tracked at 200 frames per sec for 1 sec. Parameters of sperm motility were quantified by the coordinates of sperm head for 1 sec. The following parameters were assessed, as described [18, 19]: curvilinear velocity (VCL, µm/sec) calculated by the sum of the distances along the trajectory for 1 sec; average path velocity (VAP, µm/sec), where the average path is calculated by averaging coordinates from one-sixth (33 frames) of video-frame rates; straight-line velocity (VSL, µm/sec) calculated by the straight-line distance between the first and last points of the trajectory for 1 sec; linearity (LIN, %) calculated by dividing VSL by VCL; straightness (STR, %) calculated by dividing VSL by VAP; wobble (WOB, %) calculated by dividing VAP by VCL.

Statistical analysis

Data are presented as the mean ± SEM ($n \geq 3$). Student's *t*-test was used for statistical analysis; significance was assumed at $P < 0.05$.

Results

We have already reported that the number of cauda epididymal sperm is similar between *Acrbp*$^{+/+}$ and *Acrbp*$^{-/-}$ mice [3]. To examine the abundance of *Acrbp*$^{-/-}$ mouse sperm in the female reprodutive tract, sperm were recovered from the uterus and oviduct 1.5 and 2 h after mating, respectively, and then counted (Fig. 1A). No significant difference in the number of uterine sperm was found between *Acrbp*$^{+/+}$ and *Acrbp*$^{-/-}$ mice. Interestingly, *Acrbp*$^{-/-}$ mice revealed a significant decrease in the number of oviductal sperm; the number of *Acrbp*$^{-/-}$ mouse sperm (approximately 120 cells) was considerably smaller in the oviduct of mice post mating, as compared with that of *Acrbp*$^{+/+}$ mouse sperm (more than 400 cells). These data apparently suggest that the subfertility of *Acrbp*$^{-/-}$ male mice may be attributed to the impairment in the sperm ascent from the uterus to the oviduct via the uterotubal junction.

According to already published criteria [3], *Acrbp*$^{-/-}$ mouse sperm both from the epididymis, and from the uterus and oviduct post mating were morphologically classified into four types (Supplementary Fig. 1: online only). The proportions of type-1, type-2, type-3, and type-4 epididymal sperm from *Acrbp*$^{-/-}$ mice were found to be 46, 37, 15,

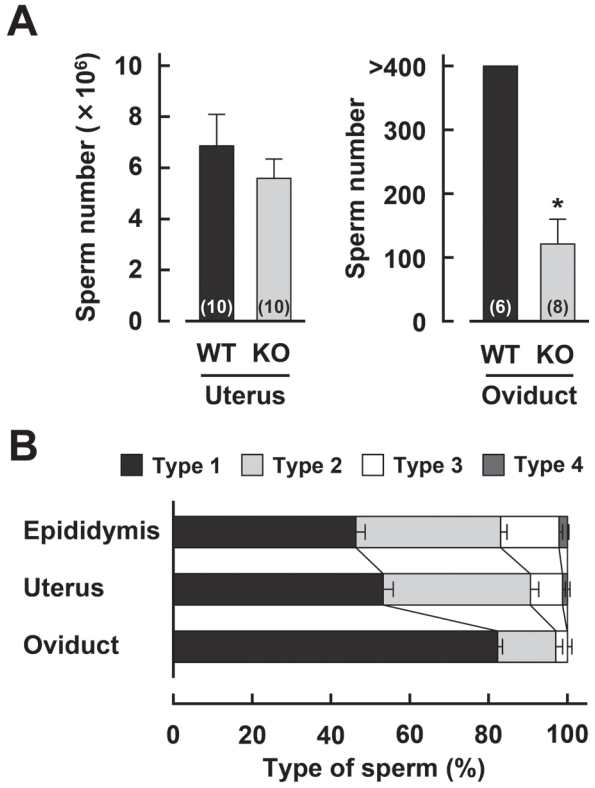

Fig. 1. Distribution of ACRBP-deficient sperm in the female reproductive tract. (A) Sperm migration into the uterus and oviduct after mating. Following mating between wild-type (WT) or ACRBP-deficient (KO) males and WT females, sperm were recovered from the uterus and oviduct 1.5 and 2 h after coitus, and then counted. Numbers in parentheses indicate the total number of uteri and oviducts examined. * $P < 0.05$. (B) Morphological distribution of KO sperm before and after mating. Sperm were recovered from the epididymis, and from the uterus and oviduct 1.5 and 4 h after mating, respectively, stained with Alexa Fluor 568-conjugated peanut agglutinin, MitoTracker Green FM, and Hoechst 33342, and then observed under a fluorescence microscope.

and 2% (53, 37, 8, and 1% for the uterine sperm), respectively (Fig. 1B). The data for epididymal sperm were essentially similar to those obtained previously [3]. More than 80% of total *Acrbp*$^{-/-}$ mouse sperm in the oviduct corresponded to type-1 sperm, whereas the proportions of type-2 and type-3 *Acrbp*$^{-/-}$ mouse sperm were approximately 15 and 3%, respectively. No type-4 *Acrbp*$^{-/-}$ mouse sperm was observed in the oviduct. Thus, *Acrbp*$^{-/-}$ mouse sperm possessing the head shape morphologically similar to that of *Acrbp*$^{+/+}$ mouse sperm may preferentially pass through the uterotubal junction. It should be noted that we did not examine the morphology of *Acrbp*$^{+/+}$ mouse sperm recovered from the uterus and oviduct after mating, because approximately 94% of epididymal sperm from *Acrbp*$^{+/+}$ mice exhibited highly uniform morphologies.

We next sought to determine whether motility of sperm deposited in the female reproductive tract differs between *Acrbp*$^{+/+}$ and *Acrbp*$^{-/-}$ mice. Following recovery of sperm from the uterus and oviduct 1.5 and 4 h after mating, respectively, the motions of sperm heads were recorded using a high-speed camera, and then analyzed using the ImageJ software (Supplementary Fig. 2: online only). Type-1 *Acrbp*$^{-/-}$ mouse sperm were morphologically indistinguishable from the type-2 sperm without staining the acrosome and nucleus. In the case of sperm recovered from the uterus, type-1/type-2 *Acrbp*$^{-/-}$ mouse sperm displayed somewhat anomalous patterns of movement trajectories as compared with *Acrbp*$^{+/+}$ mouse sperm (Supplementary Fig. 2). This may be due to irregular motility, including temporary pausing and atypical head rotation, as described previously [3]. The movement trajectories of type-3 and type-4 *Acrbp*$^{-/-}$ mouse sperm were obviously unusual, owing to the dysfunctional flagellar beating and the loss of forward movement, respectively. No remarkable difference in the trajectory was found between *Acrbp*$^{+/+}$ and type-1/type-2 *Acrbp*$^{-/-}$ mouse sperm from the oviduct (Supplementary Fig. 2).

When the movement trajectories of sperm recovered from the uterus were manually quantified by kinetic analysis, type-1/type-2 *Acrbp*$^{-/-}$ mouse sperm were comparable with *Acrbp*$^{+/+}$ mouse sperm in the values of VCL, VSL, and VAP (Fig. 2). The velocity ratios, LIN and WOB in type-1/type-2 *Acrbp*$^{-/-}$ mouse sperm, however, were significantly lower than those in *Acrbp*$^{+/+}$ mouse sperm. As expected, all parameters of type-3 and type-4 *Acrbp*$^{-/-}$ mouse sperm, except for STR, were affected. No significant difference in the kinetic parameters was found between *Acrbp*$^{+/+}$ and *Acrbp*$^{-/-}$ mouse sperm recovered from the oviduct (Fig. 2). These results suggest that *Acrbp*$^{-/-}$ mouse sperm, which have already migrated into the ovary, retain the normal motility.

To visualize the migration of *Acrbp*$^{-/-}$ mouse sperm from the uterus to the ampulla, transgenic mice expressing enhanced green fluorescent protein (EGFP) and red fluorescent protein (RFP) in the acrosome and mitochondria of sperm, respectively [13], were crossed with *Acrbp*$^{-/-}$ mice to obtain *Tg*$^{+/-}$/*Acrbp*$^{-/-}$ mice. Superovulated wild-type mice were mated with *Tg*$^{+/-}$/*Acrbp*$^{+/+}$ or *Tg*$^{+/-}$/*Acrbp*$^{-/-}$ males; thereafter, the intact oviduct was pulled out from the mice 6 h after mating, and observed under a fluorescence microscope. As illustrated in Fig. 3A, we divided the oviduct into seven regions (R1–R7), where the lower isthmus corresponded to R1 and R2, and the ampulla corresponded to R7 [8, 10]. When the number of sperm in each region was counted, more than 200 *Tg*$^{+/-}$/*Acrbp*$^{+/+}$ mouse sperm were observed in R1, and the sperm number decreased with increasing distance from R1 (Fig. 3A). Approximately 20 *Tg*$^{+/-}$/*Acrbp*$^{+/+}$ mouse sperm were present in R7. Consistent with the data indicated in Fig. 1A, *Tg*$^{+/-}$/*Acrbp*$^{-/-}$ males exhibited a significant decrease in the number of sperm in R1, R2, R3, and R7.

We also classified fertilizing sperm in R7 into three types based on the distance between the oocyte and sperm, as follows: type a, a sperm present on the oocyte zona pellucida (ZP) or already fertilized with the oocyte; type b, a sperm localized within a 100-μm distance from the ZP; type c, a sperm present in the cumulus mass but absent within the 100-μm distance from the ZP (Fig. 3B). Interestingly, *Tg*$^{+/-}$/*Acrbp*$^{-/-}$ mouse sperm were characterized by increased proportions of type-b and type-c sperm (Supplementary Fig. 3: online only). Since the motility of *Acrbp*$^{-/-}$ mouse sperm recovered from the oviduct is comparable with that of *Acrbp*$^{+/+}$ mouse sperm (Fig. 2), the loss of ACRBP may result in a marked reduction in the ability to successfully gain access to the unfertilized oocytes. Notably, no

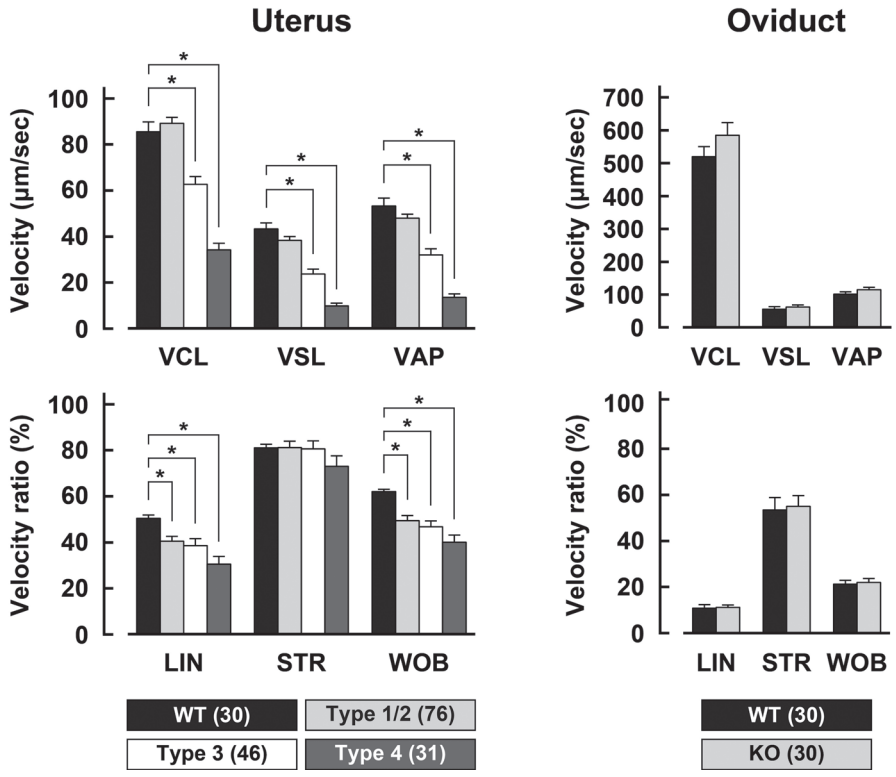

Fig. 2. Motility of sperm recovered from the uterus and oviduct. Values of the parameters, VCL (curvilinear velocity), VAP (average path velocity), VSL (straight-line velocity), LIN (linearity), STR (straightness), and WOB (wobble), were calculated from the trajectories of wild-type (WT) and ACRBP-deficient (KO) sperm. Numbers in parentheses indicate the total number of sperm examined. * $P < 0.05$.

sperm containing EGFP in the acrosome was observed in R7 in both $Tg^{+/-}/Acrbp^{+/+}$ and $Tg^{+/-}/Acrbp^{-/-}$ mice.

Discussion

Here, we describe the behavior of $Acrbp^{-/-}$ mouse sperm in the female reproductive tract. Despite intensive efforts, the mechanism of sperm migration through the female reproductive tract remains poorly understood yet; how do uterine sperm enter into and pass through the uterotubal junction? How do sperm gain access to the unfertilized oocytes? As shown in Fig. 1A, $Acrbp^{-/-}$ male mice exhibited a significant reduction in the number of sperm that migrated from the uterus to the oviduct via the uterotubal junction. We also found that more than 80% of total $Acrbp^{-/-}$ mouse sperm that migrated to the oviduct correspond to type-1 sperm (approximately 95% for type-1 and type-2 sperm, see Fig. 1B). Since the motility of type-1/type-2 $Acrbp^{-/-}$ mouse sperm recovered from the oviduct was closely similar to that of $Acrbp^{+/+}$ mouse sperm, it is possible that sperm motility is required for the passage of uterine sperm through the uterotubal junction. However, this possibility appears to be inconsistent with the recent observation [9] indicating that sperm motility is not sufficient for successful entry of sperm into the uterotubal junction. In contrast, regardless of sperm motility, myosalpinx contractions may participate in the transport of sperm from the uterus to the uterotubal junction and subsequently to the isthmus [10], as described above. In addition, the uterotubal junction has been suggested to function as a barrier against morphologically abnormal sperm [20]. Further studies are needed to elucidate the mechanism of sperm passage through the uterotubal junction, although the present study assumes the presence of an unknown selection mechanism by which morphologically abnormal sperm are eliminated during the process of sperm entry into the uterotubal junction.

Previously, we found that the transport of sperm as a tight assemblage from the lower isthmus (R1 and R2 in Fig. 3A) to the middle isthmus (R3 and R4) predominantly depends on oviductal fluid flows produced by myosalpinx contractions, while sperm migration to the ampulla (R7) is achieved by sperm flagellar motility in the middle and/or upper (R5 and R6) isthmus [10]. As reported by other workers [8, 9, 11], sperm in the lower isthmus are mostly acrosome-intact, and very few sperm, which have already undergone the acrosome reaction, migrate into the ampulla. Moreover, when an oocyte in the ampulla is already fertilized, the sperm swims away from the fertilized oocyte to interact with unfertilized oocytes [11]. In the present study, we confirmed that no sperm containing EGFP in the acrosome from both $Tg^{+/-}/Acrbp^{+/+}$ and $Tg^{+/-}/Acrbp^{-/-}$ mice is present in the ampulla, as described above. Although motility of oviductal sperm is similar between $Acrbp^{+/+}$ and $Acrbp^{-/-}$ mice (Fig. 2), $Tg^{+/-}/Acrbp^{-/-}$ mouse sperm are characterized by increased proportions of type-b and type-c sperm (Fig. 3B and Supplementary Fig. 3). It is thus conceivable that $Acrbp^{-/-}$ mouse sperm possess remarkably reduced ability to recognize

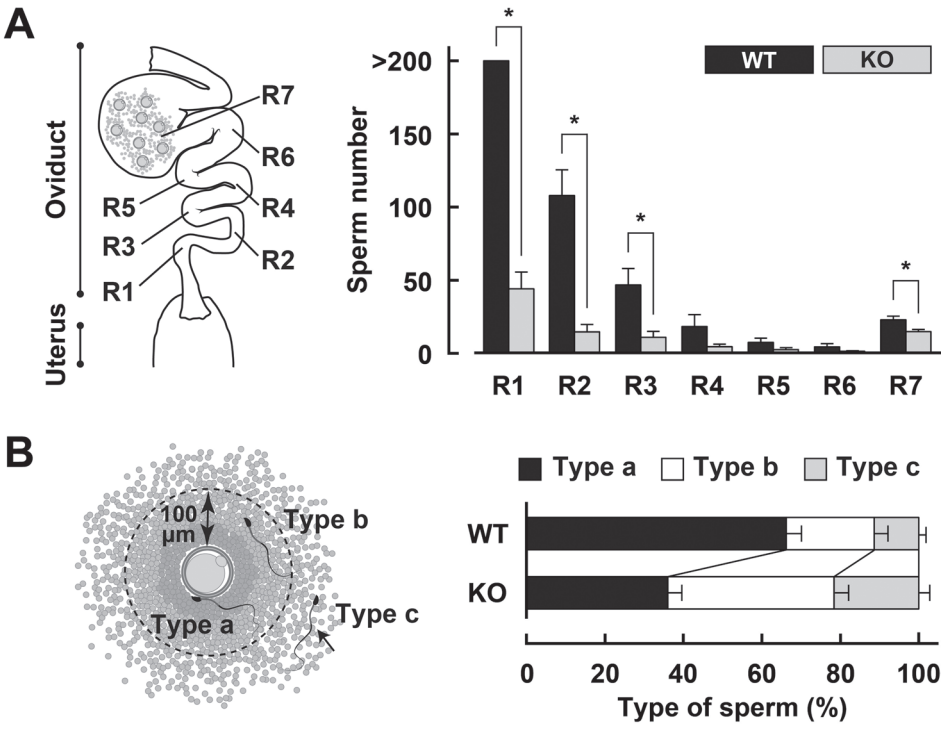

Fig. 3. Behavior of fertilizing sperm in the oviduct. (A) Regional distribution of sperm in the oviduct. Female mice were mated with $Tg^{+/-}/Acrbp^{+/+}$ (WT) or $Tg^{+/-}/Acrbp^{-/-}$ (KO) mice, and the numbers of sperm in the regions R1–R7 were counted 6 h after mating. More than 8 oviducts were examined for each of the WT and KO mice. * $P < 0.05$. (B) Sperm behavior in the ampulla. Fertilizing sperm in R7 were classified into three types according to the distance between the oocyte and sperm, as follows: type a, a sperm present on the oocyte zona pellucida or already fertilized with the oocyte; type b, a sperm localized within a 100-μm distance from the zona pellucida; type c, a sperm present in the cumulus mass but absent within the 100-μm distance from the zona pellucida. Fifteen oviducts were examined for each of WT and KO mouse sperm.

the unfertilized oocytes in the cumulus mass. Even if both $Acrbp^{+/+}$ and type-1/type-2 $Acrbp^{-/-}$ mouse sperm exhibit close similarities in morphology and motility (Supplementary Figs. 1 and 2, and Fig. 2), the mutant sperm may fail to properly display a possible regulatory molecule that is capable of recognizing the unfertilized oocytes on the sperm surface after acrosomal exocytosis.

$Acrbp^{-/-}$ male mice show a severely reduced fertility, and the litter sizes in the crosses between $Acrbp^{-/-}$ males and $Acrbp^{+/+}$ females dramatically decreases, as described before [3]. We initially believed that this decrease reflects the impairment in the migration of $Acrbp^{-/-}$ mouse sperm from the uterus to the oviduct via the uterotubal junction (Fig. 1A). However, our data suggest that male subfertility of $Acrbp^{-/-}$ mice may be explained by the incompleteness of the acrosome reaction rather than the reduced number of sperm migrated into the oviduct. Our future studies will focus on the interaction between the acrosome-reacted sperm and unfertilized or fertilized oocytes in the cumulus mass.

Acknowledgements

We thank Drs M Okabe and M Ikawa, and RIKEN BioResource Center for providing transgenic mice, and Drs S Kashiwabara, Y Kanemori, and Y Ishikawa-Yamauchi for their help in the preparation of the manuscript. This work was supported in part by a grant from Japan Society for the Promotion of Science to TB.

References

1. **Baba T, Niida Y, Michikawa Y, Kashiwabara S, Kodaira K, Takenaka M, Kohno N, Gerton GL, Arai Y.** An acrosomal protein, sp32, in mammalian sperm is a binding protein specific for two proacrosins and an acrosin intermediate. *J Biol Chem* 1994; **269**: 10133–10140. [Medline]
2. **Kanemori Y, Ryu JH, Sudo M, Niida-Araida Y, Kodaira K, Takenaka M, Kohno N, Sugiura S, Kashiwabara S, Baba T.** Two functional forms of ACRBP/sp32 are produced by pre-mRNA alternative splicing in the mouse. *Biol Reprod* 2013; **88**: 105. [Medline] [CrossRef]
3. **Kanemori Y, Koga Y, Sudo M, Kang W, Kashiwabara S, Ikawa M, Hasuwa H, Nagashima K, Ishikawa Y, Ogonuki N, Ogura A, Baba T.** Biogenesis of sperm acrosome is regulated by pre-mRNA alternative splicing of Acrbp in the mouse. *Proc Natl Acad Sci USA* 2016; **113**: E3696–E3705. [Medline] [CrossRef]
4. **Baba T, Azuma S, Kashiwabara S, Toyoda Y.** Sperm from mice carrying a targeted mutation of the acrosin gene can penetrate the oocyte zona pellucida and effect fertilization. *J Biol Chem* 1994; **269**: 31845–31849. [Medline]
5. **Yao R, Ito C, Natsume Y, Sugitani Y, Yamanaka H, Kuretake S, Yanagida K, Sato A, Toshimori K, Noda T.** Lack of acrosome formation in mice lacking a Golgi protein, GOPC. *Proc Natl Acad Sci USA* 2002; **99**: 11211–11216. [Medline] [CrossRef]
6. **Lin YN, Roy A, Yan W, Burns KH, Matzuk MM.** Loss of zona pellucida binding proteins in the acrosomal matrix disrupts acrosome biogenesis and sperm morphogenesis. *Mol Cell Biol* 2007; **27**: 6794–6805. [Medline] [CrossRef]
7. **Fujihara Y, Satouh Y, Inoue N, Isotani A, Ikawa M, Okabe M.** SPACA1-deficient male mice are infertile with abnormally shaped sperm heads reminiscent of globozoospermia. *Development* 2012; **139**: 3583–3589. [Medline] [CrossRef]
8. **La Spina FA, Puga Molina LC, Romarowski A, Vitale AM, Falzone TL, Krapf D, Hirohashi N, Buffone MG.** Mouse sperm begin to undergo acrosomal exocytosis in the

upper isthmus of the oviduct. *Dev Biol* 2016; **411**: 172–182. [Medline] [CrossRef]
9. **Muro Y, Hasuwa H, Isotani A, Miyata H, Yamagata K, Ikawa M, Yanagimachi R, Okabe M.** Behavior of mouse spermatozoa in the female reproductive tract from soon after mating to the beginning of fertilization. *Biol Reprod* 2016; **94**: 80. [Medline] [CrossRef]
10. **Ishikawa Y, Usui T, Yamashita M, Kanemori Y, Baba T.** Surfing and swimming of ejaculated sperm in the mouse oviduct. *Biol Reprod* 2016; **94**: 89. [Medline] [CrossRef]
11. **Hino T, Muro Y, Tamura-Nakano M, Okabe M, Tateno H, Yanagimachi R.** The behavior and acrosomal status of mouse spermatozoa in vitro, and within the oviduct during fertilization after natural mating. *Biol Reprod* 2016; **95**: 50. [Medline] [CrossRef]
12. **Wang S, Larina IV.** In vivo three-dimensional tracking of sperm behaviors in the mouse oviduct. *Development* 2018; **145**: dev157685. [Medline] [CrossRef]
13. **Hasuwa H, Muro Y, Ikawa M, Kato N, Tsujimoto Y, Okabe M.** Transgenic mouse sperm that have green acrosome and red mitochondria allow visualization of sperm and their acrosome reaction in vivo. *Exp Anim* 2010; **59**: 105–107. [Medline] [CrossRef]
14. **Kawano N, Kang W, Yamashita M, Koga Y, Yamazaki T, Hata T, Miyado K, Baba T.** Mice lacking two sperm serine proteases, ACR and PRSS21, are subfertile, but the mutant sperm are infertile in vitro. *Biol Reprod* 2010; **83**: 359–369. [Medline] [CrossRef]
15. **Yamashita M, Honda A, Ogura A, Kashiwabara S, Fukami K, Baba T.** Reduced fertility of mouse epididymal sperm lacking Prss21/Tesp5 is rescued by sperm exposure to uterine microenvironment. *Genes Cells* 2008; **13**: 1001–1013. [Medline] [CrossRef]
16. **Toyoda Y, Yokoyama M, Hoshi T.** Studies on fertilization of mouse eggs in vitro. *Jpn J Anim Reprod* 1971; **16**: 152–157. [CrossRef]
17. **Yamazaki T, Yamagata K, Baba T.** Time-lapse and retrospective analysis of DNA methylation in mouse preimplantation embryos by live cell imaging. *Dev Biol* 2007; **304**: 409–419. [Medline] [CrossRef]
18. **Wilson-Leedy JG, Ingermann RL.** Development of a novel CASA system based on open source software for characterization of zebrafish sperm motility parameters. *Theriogenology* 2007; **67**: 661–672. [Medline] [CrossRef]
19. **Mortimer ST.** A critical review of the physiological importance and analysis of sperm movement in mammals. *Hum Reprod Update* 1997; **3**: 403–439. [Medline] [CrossRef]
20. **Krzanowska H.** The passage of abnormal spermatozoa through the uterotubal junction of the mouse. *J Reprod Fertil* 1974; **38**: 81–90. [Medline] [CrossRef]